ACS OMEGA

http://pubs.acs.org/journal/acsodf

Article

Preparation of a Gangue-Based X-type Zeolite Molecular Sieve as a Multiphase Fenton Catalyst and Its Catalytic Performance

MiaoSen Zhang and XiaoLi Wang*

Cite This: *ACS Omega* 2021, 6, 18414−18425

Read Online

ACCESS | Metrics & More | Article Recommendations

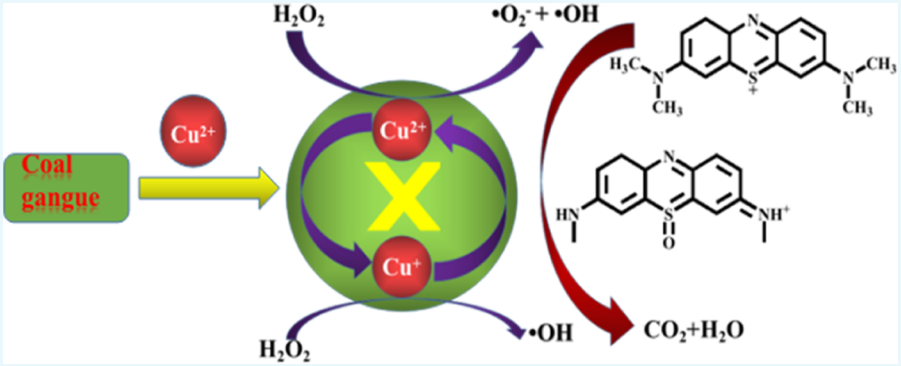

ABSTRACT: In this study, a series of X-type zeolite molecular sieve catalysts, modified with copper (Cu-X), were prepared by an alkali fusion−hydrothermal synthesis using coal gangue from Inner Mongolia. These catalysts were used in the degradation of the methylene blue dye by a Fenton-like reaction. Characterization results showed that Cu is considered to be present in the surface structure of the zeolite in the form of doped Cu ions and metal oxide. It is believed that Cu^{2+} is the main active site involved in the Fenton reaction. The X-ray photoelectron spectroscopy (XPS) spectra indicated that Cu^{2+} and Cu^+ coexist in the catalysts and participate together in the Fenton reaction. The degradation of methylene blue by the Cu-X catalysts was investigated to determine the optimal catalytic conditions in terms of six aspects: catalyst dosage, initial solution concentration, initial pH of the solution, H_2O_2 dosage, copper loading, and reaction temperature. The experimental results showed that CX-1.0 had excellent activity and stability for the degradation and decolorization of the methylene blue dye, which could completely degrade the dye within 90 min, and the total organic carbon removal rate reached as high as 97.8%. Electron spin resonance (ESR) and radical capture experiments showed that $^\bullet$OH played a dominant role in the Fenton-like reaction. Combined with XPS, ESR, and catalytic tests, the redox cycle of Cu^+/Cu^{2+} was found to be accelerating the generation of reactive radicals in the Fenton system.

1. INTRODUCTION

Coal gangue is a byproduct of coal mining and processing, which is unavoidable due to limitations of the existing technical conditions, and emissions are on the rise.[1] The accumulation and storage of coal gangue occupy a large amount of land area. Gangue is prone to spontaneous combustion, and the pollutants contained within will pollute the environment after emission.[2]

With science and technological advancements, the utilization of coal gangue has also been increasingly developed from simple uses to the extraction of useful elements. Therefore, the synthesis of zeolites using coal gangue is a more efficient way to use the effective components in coal gangue. Generally speaking, the total amount of SiO_2 and Al_2O_3 in coal gangue can reach 65−95%, which provides the required silicon source and aluminum source for the synthesis of zeolites and is the theoretical basis for using coal gangue as a raw material.[3]

The wastewater from printing and dyeing is common in various industrial processes, leading to the generation of large amounts of wastewater contaminated with these chemicals. Methylene blue [3,7-*bis*(dimethylamino)phenothiazin-5-ium chloride, MB] is one of the commonly used dyes.[4] It is widely used in the textile, paper, plastic, leather, food, and cosmetic industries. With the rapid development of the textile printing and dyeing industry, more and more important commercial dyes are being discharged into bodies of water in different ways.[5] MB can cause burning eye pain and may lead to eye

Received: May 11, 2021
Accepted: June 23, 2021
Published: July 2, 2021

damage. Also, when inhaled, it may cause short-term rapid breathing or difficulty in breathing. At the same time, it may lead to nausea, vomiting, profuse sweating, confusion, and hemoglobinemia.[6,7] Therefore, before discharging the methylene blue dye wastewater, it should be effectively treated to remove methylene blue from the wastewater to try to avoid its release into the environment. Therefore, the removal of dye wastewater has also become a topic of interest for many scientific researchers, who have researched and developed many different techniques for the treatment of dye wastewater, such as physical treatment,[8] biodegradation,[9] advanced chemical oxidation,[10] and photocatalytic degradation.[11−13]

As for advanced oxidation processes (AOPs) as a chemical treatment method, researchers have targeted AOPs because in most cases, they show process flexibility, efficient decomposition of organic pollutants in water, easy control of the system, mild conditions, and low cost and because importantly, they do not produce secondary pollution after the reaction.[14−16] Among them, Fenton oxidation has become the most mainstream process, which is essentially the oxidation of hydrogen peroxide by Fe^{2+} to produce hydroxyl radicals.[17] It has been widely used because it has strong oxidizing power to treat organic pollutants efficiently and has the advantages of mild conditions, low treatment cost, and simple operation.[18]

The oxidation methods discovered by the early researchers in this field were all homogeneous Fenton oxidation reactions, which can effectively treat hard-to-degrade organic pollutants in water. However, these types of reactions also have many drawbacks and shortcomings, such as low utilization of hydrogen peroxide, a narrow applicable pH range,[19,20] and generation of large amounts of iron sludge and iron salts that are difficult to recycle and reuse, which limit their application in many engineering applications.[21] As a representative advanced oxidation technology, multiphase Fenton catalytic oxidation has been widely investigated because it can compensate for many disadvantages of homogeneous Fenton materials.[22] The multiphase Fenton oxidation technology immobilizes Fe^{2+} as a catalyst on a carrier, so the solid catalyst surface provides an environment for the multiphase Fenton reaction. First, Fe^{2+} reacts with hydrogen peroxide to produce strong oxidizing hydroxyl radicals ($^{\bullet}OH$), which then oxidatively decompose the organic pollutants adsorbed on the solid surface. The $^{\bullet}OH$ radicals produced during this reaction non-selectively destroy the structure of organic pollutants, thus achieving a good degradation effect.[23,24] Compared with the homogeneous Fenton reaction, the multiphase Fenton reaction has the advantages of making the full use of hydrogen peroxide, recyclability, a wider applicable pH range, easy solid−liquid separation, and being less likely to produce iron sludge. Therefore, it has been widely studied.[25,26] Based on the multiphase Fenton reaction, researchers have found that not only the solid-phase catalysts of iron ions but also a large number of transition metal catalysts[27] (such as manganese, cobalt, copper, and so on) have good degradation performance. Since the mechanisms of these other transition metal catalysts in the degradation reaction process have similarities with the traditional multiphase Fenton reaction, people call these catalysts multiphase Fenton-like oxidation techniques. Copper is an ideal substitute for iron because it exhibits a Fenton-like oxidation activity even under neutral and alkaline conditions, making copper-based Fenton-like treatment of dye wastewater feasible. The preparation of Cu-based catalysts using various carriers, including zeolites,[28,29] metal oxides,[30,31] and clays,[32,33] to participate in the Fenton-like reaction has been reported in the literature. Wang[34] *et al.* synthesized a series of Cu-based bimetallic oxides and compared their Fenton-like catalytic performance for the degradation of Orange II and ciprofloxacin. Zhang[35] *et al.* prepared smaller tunable Co_3O_4 nanoparticles on the HZSM-5 zeolite by adding various hydroxyl-rich complexing agents. Through a large number of characterization techniques and catalytic experiments, the physical and chemical properties of Co_3O_4-active components, such as crystal size, surface dispersibility, reduction, acidity, and toluene oxidation catalytic performance, have been extensively studied. Zhang[36] *et al.* prepared a series of 10% MnO_x/HZSM-5 catalysts with different zeolite Si/Al ratios by the initial impregnation method and evaluated the catalytic oxidation performance of toluene. Lu[37] *et al.* synthesized a core−shell composite of Y zeolite and a hydrophobic organic polymer (Y@St-DVB), which significantly improved the hydrophobicity and toluene adsorption capacity of Y zeolite. Modification to increase the adsorption capacity under wet conditions. Li[38] *et al.* used a ZSM-5 zeolite loaded with metal copper ions for Fenton-like catalytic degradation of phenol.

These previous studies have focused on the loading of metallic copper on different carriers to improve the activity and stability of the catalysts and to minimize the negative effects from the homogeneous Fenton reaction. Zeolites are mainly composed of silica-aluminates and have a reticulated internal space structure with a large number of uniformly sized pore channels, and their structure makes them ideal carriers for loading transition metals, along with their adsorption, catalytic, and ion selectivity characteristics.[38]

Thus, in this study, for the first time, the mined solid waste coal gangue stone X-type zeolite molecular sieve was used as a carrier and modified with Cu to obtain a Fenton-based catalyst, Cu-X, which was applied to the catalytic degradation of methylene blue dye wastewater. Compared with iron, copper has the advantages of a wider applicable pH range, easy solid−liquid separation, and difficulty in producing iron sludge. This process is a typical example of waste-to-waste, where waste is treated with other waste, which has not been extensively studied. In this study, the relevant physicochemical characterizations of the catalyst were determined. To obtain the optimal catalytic conditions, the effects of Cu loading, catalyst dosage, H_2O_2 dosage, dye concentration, temperature, and pH on the dye degradation rate were investigated. Also, the roles of the reactive radicals in the Fenton-like reaction and the catalytic mechanism were investigated.

2. RESULTS AND DISCUSSION

2.1. Catalyst Characterization. *2.1.1. X-ray Diffraction Analysis.* Figure 1 shows the X-ray diffraction (XRD) patterns of the X-type zeolite and X-type zeolites with different Cu loadings. It can be seen from Figure 1 that these spectra show peaks that belong to the X-type zeolite structure. However, when the Cu content is higher than 1.0 g/L, the zeolite peak intensity is weakened, which proves that the Cu modification had some effect on the zeolite structure, indicating that Copper in the form of Cu^{2+} or Cu^{+} cations is located in zeolites in channels in the so-called ion-exchange positions. With this content, a very small part of copper can be in the form of polyoxocations.[39,40] Compared to that of the pure X-type zeolite, the 2θ angle of each diffraction peak shifts toward somewhat higher values with the increasing Cu content, also

https://doi.org/10.1021/acsomega.1c02469
ACS Omega 2021, 6, 18414−18425

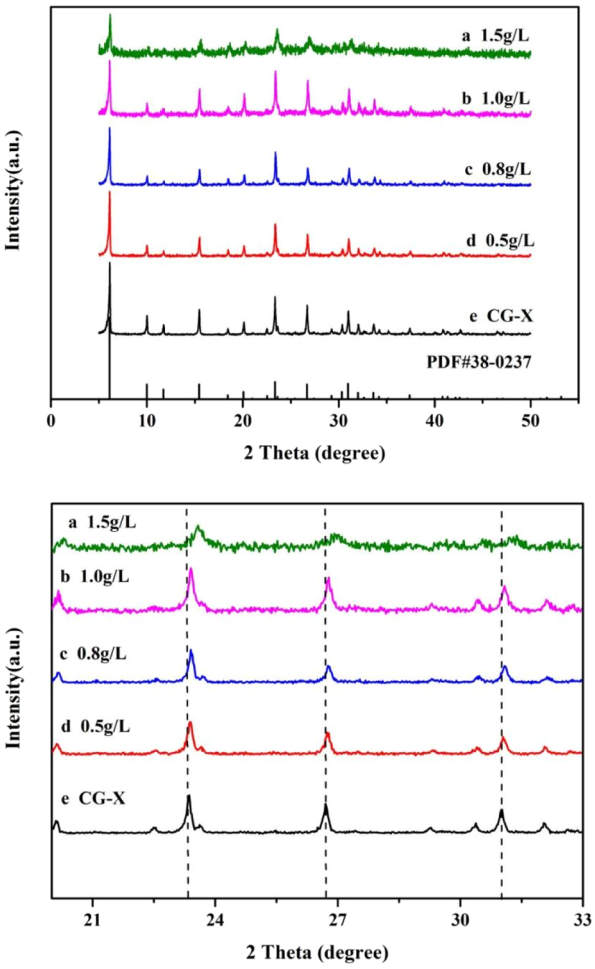

Figure 1. XRD patterns of CG-X and Cu-X with different copper contents.

proving that the addition of Cu affects the crystal structure of the zeolite. Previous studies have pointed out that the shift of the diffraction peak means that Cu^{2+} occupies the Na and Al sites in the structure. Cu is considered to be present in the surface structure of the zeolite in the form of doped Cu ions and metal oxide.

2.1.2. Nitrogen Sorption Analysis. Figure 2 shows the N_2 adsorption and desorption isotherms of the pure X-type zeolite and CX-1.0. The relevant parameters of the Brunauer–Emmett–Teller (BET) isotherm are shown in Table 1. The

Table 1. Parameters of the Surface Structure of Zeolite X and CX-1.0

	surface area/(m^2/g)	pore volume/(cm^3/g)
sample	S_{BET}	V_{total}
zeolite X	511.2	0.31
CX-1.0	381.5	0.28

isotherms of the pure X-type zeolite and CX-1.0 were typical type IV isotherms, and the H4 hysteresis loop was closed at a P/P_0 value of about 0.4. The specific surface area (S_{BET}) of pure zeolite X was 511.2 m^2/g, and the pore volume was 0.31 cm^3/g. The S_{BET} of the CX-1.0 sample was 381.5 m^2/g, and the pore volume was 0.28 cm^3/g. The hysteresis loop is a mesopore between aggregated zeolite crystals.[41] Replacing two Na^+ cations by one Cu^{2+} cation should lead to more open pores. At the same time, a slight decrease in the specific surface area may be due to an increase in the molecular weight of the sorbent ($64 > 2 \times 23$). V_{total}, as follows from Figure 2, does not increase, but it decreases. The adsorption–desorption isotherms show that the pore structure of the X zeolite mostly maintained its original structure, even after Cu modification.

2.1.3. Scanning Electron Microscopy Analysis. Figure 3a shows the scanning electron microscopy (SEM) image of the coal gangue powder. This shows that the surfaces of the coal gangue particles were rough, loose, irregular, and in the shape of lamellae. This was because of kaolinite, the main mineral component of coal gangue. The structural hydroxyl groups of kaolinite were distributed in the aluminum–oxygen octahedral layer, providing the possibility of preparing zeolites from coal gangue.[42]

Figure 3b,c shows the SEM images of the pure X-type zeolite. Figure 3d shows the SEM image of CX-1.0. It can be seen from the figures that the synthesized zeolites are high-quality, octahedral-structured X-type zeolites with a complete crystalline shape and well-defined angles. The pure X-type zeolite consisted mainly of large particles (2–4 μm) aggregated in cuboidal-like layered crystals. After Cu modification, the

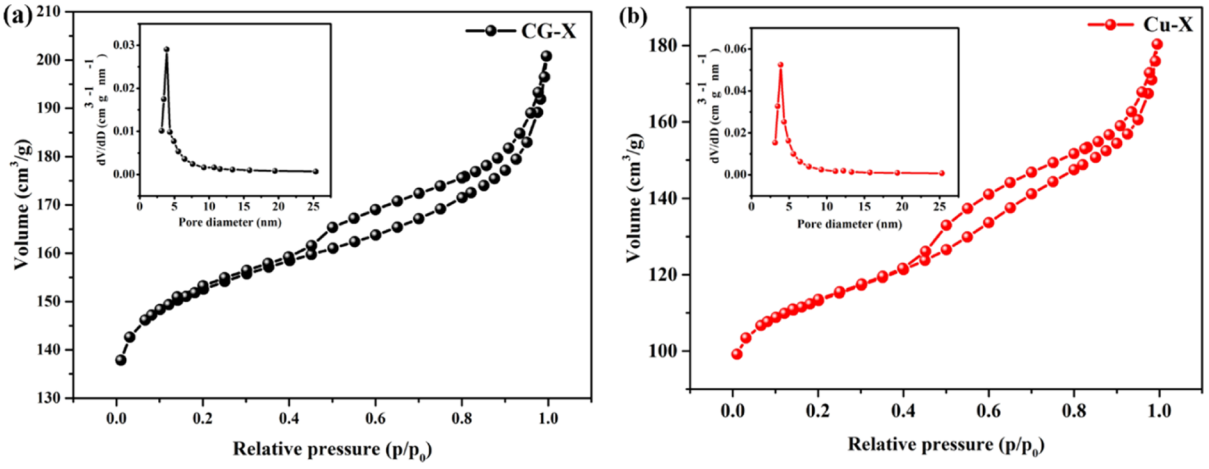

Figure 2. N_2 adsorption–desorption isotherms of CG-X (a) and CX-1.0 (b).

https://doi.org/10.1021/acsomega.1c02469
ACS Omega 2021, 6, 18414–18425

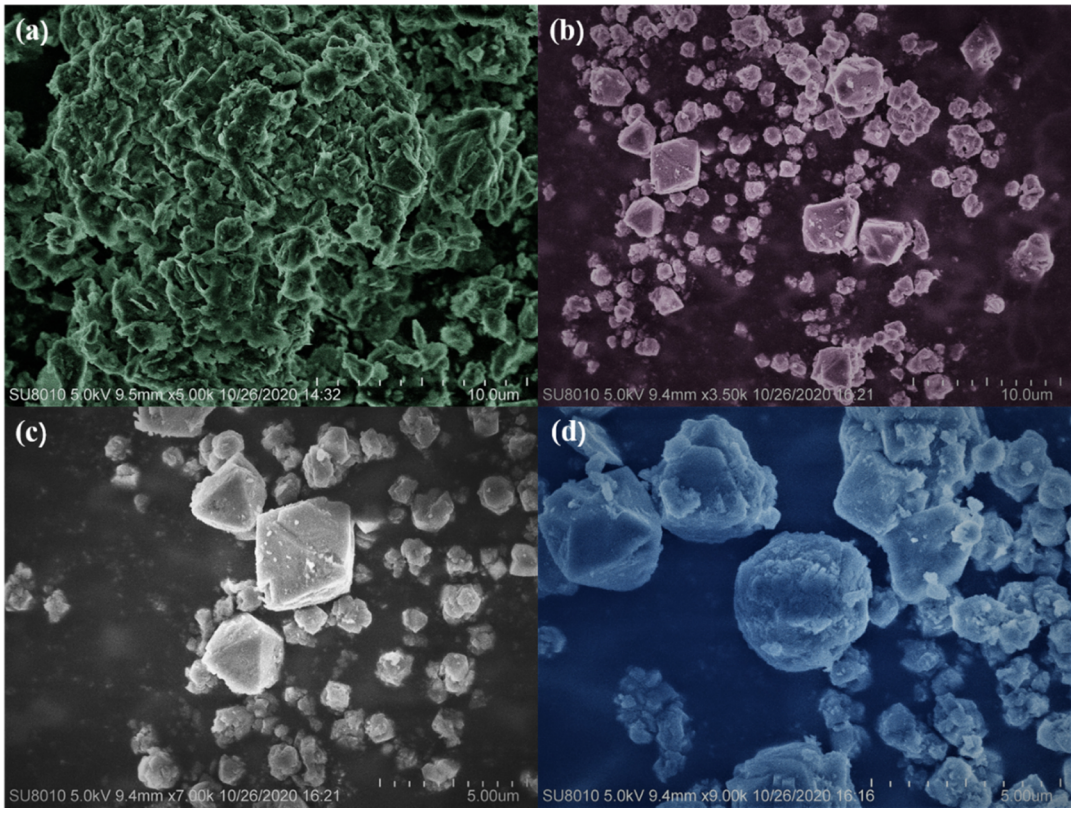

Figure 3. SEM images of coal gangue (a), CG-X (b,c), and CX-1.0 (d).

morphology of the CX-1.0 sample was the same, but the copper wrapping on its surfaces can be seen.

2.1.4. Transmission Electron Microscopy Analysis. Figure 4 shows the transmission electron microscopy (TEM) images of CG-X and CX-1.0. The clear morphology and well-defined edges of pure CG-X and CX-1.0 demonstrated their high crystallinity, which was consistent with the XRD results. The high-resolution TEM (HRTEM) images of CG-X and CX-1.0 show distinct lattice stripes, indicating the high crystallinity of the synthesized CG-X and CX-1.0. However, no copper particles were observed, indicating that copper is well dispersed in the form of amorphous metal or aggregated into microcrystals with too small grains. The HRTEM image in Figure 4g shows a lattice stripe with a distance of 0.351 nm from the crystal plane, which corresponds to the (7 1 1) plane of CG-X. The HRTEM image in Figure 4h shows lattice streaks with distances of 0.477 and 0.178 nm from the crystal plane, corresponding to the (5 1 1) and (13 5 1) planes of CX-1.0, respectively. This indicates that the crystal boundaries of CX-1.0 are clear and the Cu modification has little effect on the crystallinity of the X-type zeolite.

2.1.5. X-ray Photoelectron Spectroscopy Analysis. X-ray photoelectron spectroscopy (XPS) has been commonly used to study the elemental composition, as well as the content, of various compounds. Figure 5 shows the XPS spectra of the pure X-type zeolite and CX-1.0 catalysts before and after the Fenton-like reaction. The full XPS spectra of these three samples are shown in Figure 5a, and the presence of binding energy peaks from Cu 2p, O 1s, and C 1s can be found. Two distinct binding peaks were observed at 531.62 and 532.65 eV, attributed to Si−O and C═O, respectively, while the binding peak of Cu-X at 536.6 eV was attributed to Cu−O. Figure 5c shows six peaks in the high-resolution XPS spectra of Cu 2p for the unused and used CX-1.0 samples. The presence of Cu^{2+} was determined by the presence of peaks at 934.3 and 954.4 eV and the strong Cu^{2+} satellite peaks at 942.7 and 962.5 eV.[43]

Also, the presence of a reduced Cu (Cu^{+} or Cu^{0}) species was confirmed by the stronger peaks at binding energies of 932.8 and 952.9 eV found in fresh and used CX-1.0, respectively.[43] This phenomenon may be due to the reduction of Cu^{2+} by residual organic templates in the X-type zeolite during the heating process. It should be noted that the surface atomic ratio of Cu^{2+}/Cu^{+} changed from 4.4 for the unused Cu-X sample to 5.4 for the used Cu-X sample, which was due to the involvement of Cu^{+} and Cu^{2+} in the Fenton-like reaction. From the XPS spectra of C 1s in Figure 5d, three peaks located at 284.4, 286.0, and 288.7 eV are observed. The peaks located at 284.4 and 288.7 eV were attributed to C−C and C═C of the residual templating agents or carbon from the instrumentation and the environment.[44,45] The peak at 286.0 eV was due to C−O bonds from adsorbed CO_2.[45]

2.1.6. Fourier Transform Infrared Analysis. The infrared spectra of the pure X-type zeolite, as well as before and after the Fenton-like reaction using CX-1.0, are given in Figure 6. The absorption peaks were also analyzed, and the infrared spectra are in general agreement with the absorption peaks of the X-type zeolite.[46] The peaks appearing at around 3400 and 1633 cm^{-1} were attributed to the stretching vibration of absorbed water at the surface.[47] The peak appearing around 1000 cm^{-1} was attributed to the asymmetric stretching vibration of the Si−O−Si bond.[48] The absorption peak at 758 cm^{-1} belonged to the symmetric stretching vibration absorption peaks of the external linkage vibrations of the skeleton and the secondary structural unit (double six-membered ring) vibration absorption peaks. The peaks located at 676 cm^{-1} were attributed to internal vibrations of Si−O−Al

https://doi.org/10.1021/acsomega.1c02469
ACS Omega 2021, 6, 18414−18425

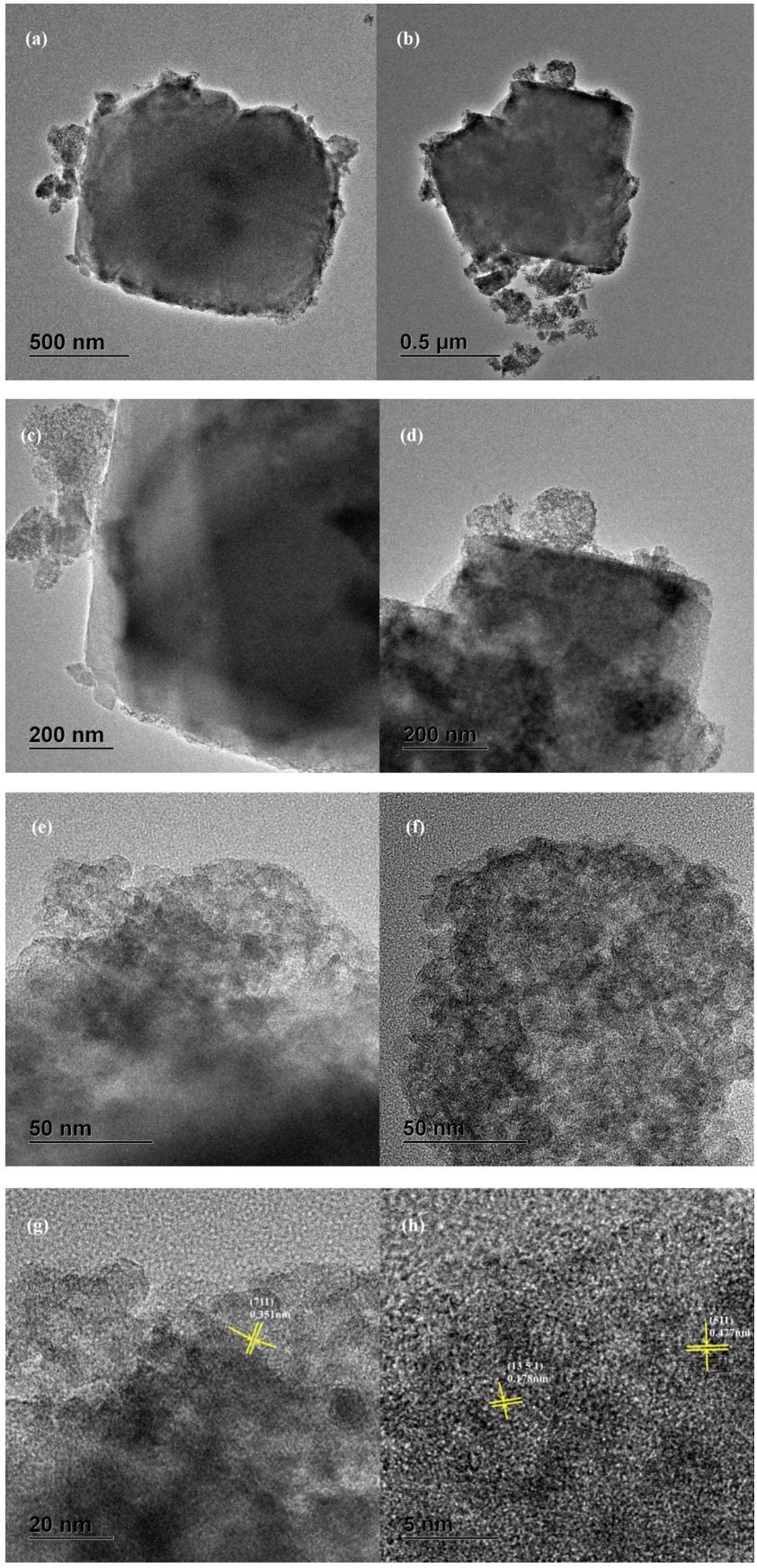

Figure 4. TEM and HRTEM images of CG-X (a,c,e,g) and CX-1.0 (b,d,f,h).

https://doi.org/10.1021/acsomega.1c02469
ACS Omega 2021, 6, 18414−18425

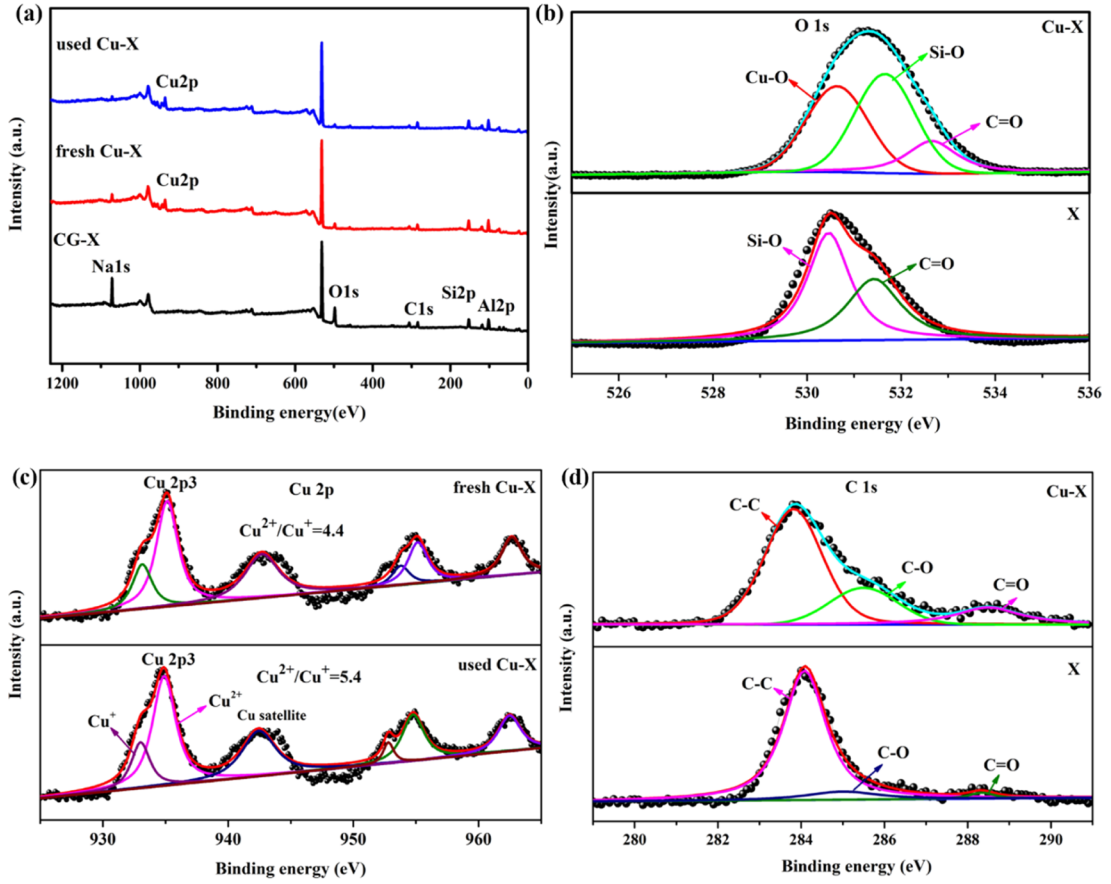

Figure 5. XPS spectra of different samples (CG-X, fresh Cu-X, and used Cu-X). XPS total spectrum (a) and high-resolution XPS spectra for O 1s (b), Cu 2p (c), and C 1s (d).

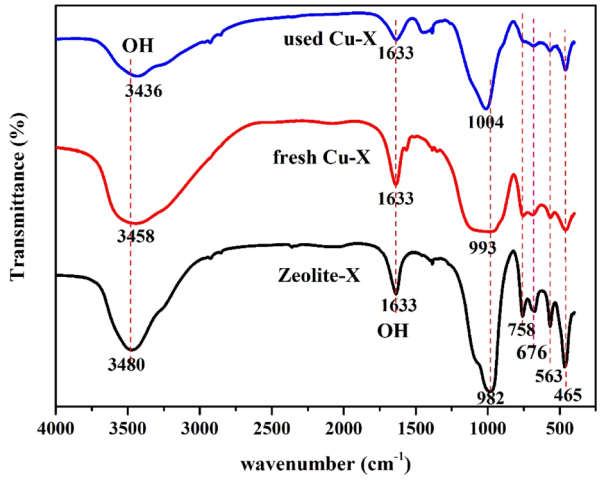

Figure 6. Infrared spectra of CG-X and CX-1.0 before and after the Fenton-like reaction.

symmetric stretching and bending. The presence of double six-membered ring vibrations and that of T−O bending vibrations were also indicated at 563 and 456 cm^{-1}, respectively.[49] After Cu modification and a Fenton-like reaction, the structure of the X-type zeolite was still well-preserved.

2.2. Catalytic Performance of CX-1.0. *2.2.1. Effect of the Concentration of the Cu^{2+} Solution for Ion-Exchange Procedures.* The addition of copper greatly improved the degradation efficiency of methylene blue. Figure 7a shows the effect of Cu-X with different copper loadings on the MB removal rate. The degradation efficiency increased with the increase in the Cu content. This phenomenon was mainly related to the increased reaction between Cu and H_2O_2 to produce $^{\bullet}OH$. The degradation rate hardly increased when the Cu loading was higher than 4%. This may be due to saturation of the Cu active sites and the scavenging effect of Cu ions on $^{\bullet}OH$ (eq 1).

$$Cu^{+} + {}^{\bullet}OH \rightarrow Cu^{2+} + OH^{-} \quad (1)$$

2.2.2. Effect of Temperature. Temperature is also a very important influence as it usually accelerates the reaction by raising the reaction rate constant. Figure 7b shows the effect of temperature on the catalytic performance. The degradation efficiency was optimal when the temperature reached 60 °C and then remained constant with the increasing temperature to reach 100% within 60 min. The slow increase in the high-temperature catalytic efficiency may be related to the decomposition of a large excess of H_2O_2 at these temperatures because the more likely unproductive degradation of H_2O_2 takes place, which results in a smaller number of radicals.[50] Based on the combination of degradation efficiency and high-temperature energy consumption, the optimal degradation temperature of the Cu-X catalyst for methylene blue was 60 °C. Meanwhile, the degradation efficiency showed a significant increasing trend with time and remained constant after about 60 min (close to 100% degradation efficiency).

2.2.3. Effect of the Dosing Amount. The effect of catalyst dosage on the degradation efficiency was similar to that of the

https://doi.org/10.1021/acsomega.1c02469
ACS Omega 2021, 6, 18414−18425

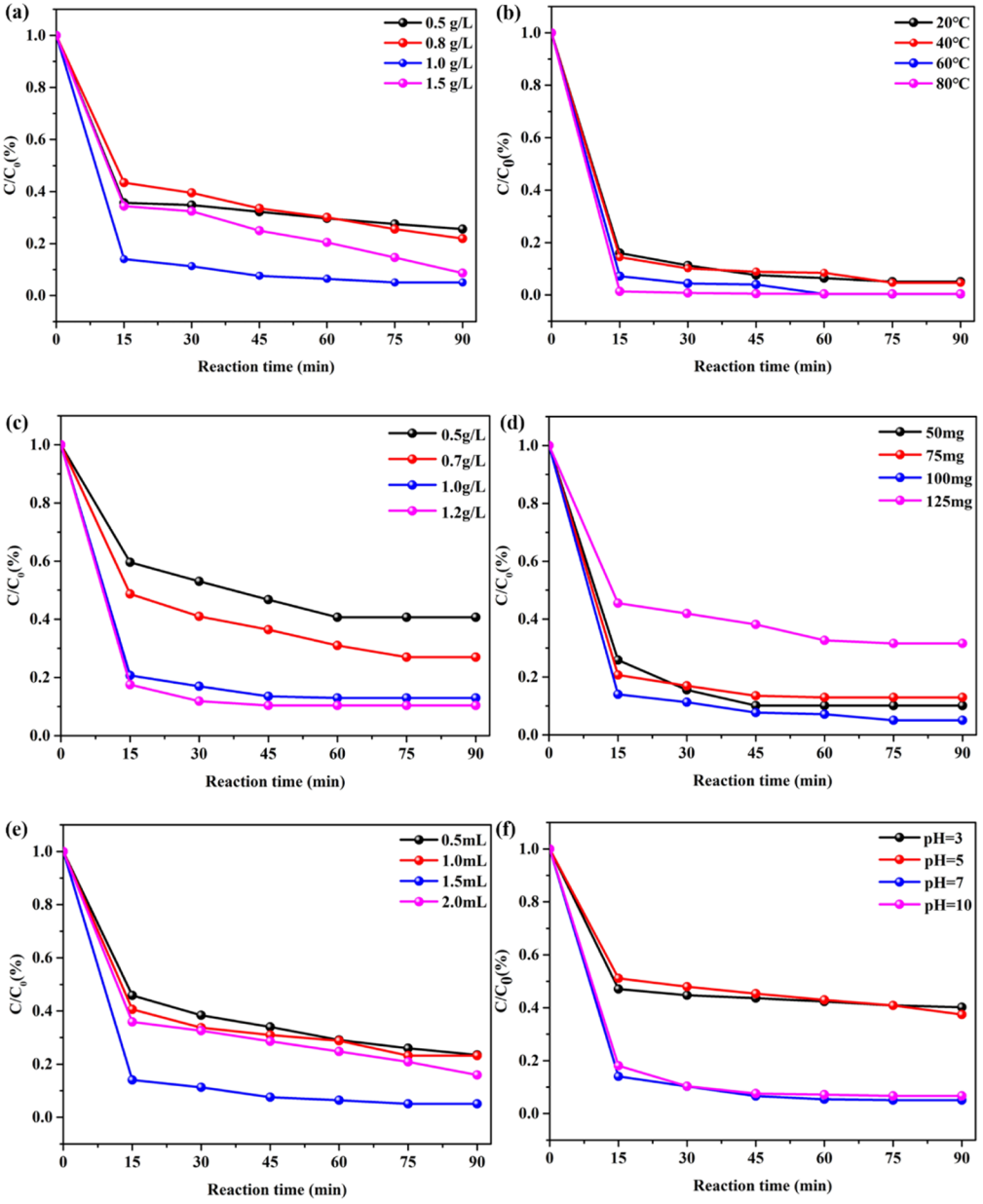

Figure 7. Effect of different parameters on the degradation fraction of methylene blue: the concentration of Cu^{2+} solution for ion-exchange procedures (a), temperature (b), dosing amount (c), dye concentration (d), H_2O_2 dosage (e), and pH (f).

loading amount. As shown in Figure 7c, the degradation efficiency remained constant for 60 min at a catalyst dosage of 1.0 g/L (close to 100% degradation efficiency). When the catalyst reached a certain amount, the amount of methylene blue captured at the active sites of the catalyst no longer increased. The optimum catalyst dosage for the degradation of methylene blue by the Fenton-like reaction using the Cu-X catalyst was 1.0 g/L, under the premise of reducing the operating cost.

2.2.4. Effect of Dye Concentration. Methylene blue concentration and H_2O_2 dosage are closely related, as shown in Figure 7d. The decrease in the methylene blue concentration implied an increase in the relative amount of H_2O_2. Therefore, when the methylene blue concentration was low, the degradation rate also decreased. With the increase in the methylene blue concentration, the degradation rate also improved, but with the further increase in the methylene blue concentration, the degradation rate decreased, which was mainly related to the insufficient amount of H_2O_2 and the amount of the catalyst.

2.2.5. Effect of H_2O_2 Dosage. H_2O_2 also plays an important role in the Fenton-like catalytic reaction. Figure 7e illustrates the effect of the H_2O_2 dosage (0.5−2.0 mL) on the degradation efficiency of methylene blue. When the H_2O_2 dosage was 1.5 mL, the methylene blue removal rate was 99.7%. When the amount of H_2O_2 was increased to 2.0 mL, the methylene blue removal rate decreased to 80.1%. The decrease in the removal rate may be related to excess H_2O_2 reacting with reactive hydroxyl radicals to form perhydroxyl radicals ($HO_2^{\bullet}$), which has almost no positive effects in the Fenton-like process (eqs 2−5).[51,52] Therefore, this Fenton-like reaction requires an appropriate H_2O_2 concentration.

$$^{\bullet}OH + H_2O_2 \rightarrow HO_2^{\bullet} + H_2O \quad (2)$$

https://doi.org/10.1021/acsomega.1c02469
ACS Omega 2021, 6, 18414−18425

$$2^{\bullet}OH \rightarrow H_2O_2 \quad (3)$$

$$HO_2^{\bullet} + {}^{\bullet}OH \rightarrow H_2O + O_2 \quad (4)$$

$$2HO_2^{\bullet} \rightarrow H_2O_2 + O_2 \quad (5)$$

2.2.6. Effect of the Initial pH of the Solution. The initial pH also plays an important role in the degradation of methylene blue. The solution pH affects the decomposition rate of H_2O_2 and the surface charge of the catalyst. Therefore, the effect of the initial solution pH on the degradation efficiency of methylene blue was investigated and is shown in Figure 7f. The degradation rate of methylene blue was sensitive to pH under alkaline and neutral conditions and reached the maximum value under both conditions. At lower pH, more H^+ was generated, which can react with $^{\bullet}OH$. This means that more reactive $^{\bullet}OH$ radicals were consumed,[50] which hindered the reaction of Cu with H_2O_2 and reduced the rate of $^{\bullet}OH$ production. Also, the active centers of the catalyst were usually unstable in acidic media.[53] Therefore, acidic conditions are not favorable for the degradation of methylene blue using Fenton-like reactions with the Cu-X catalysts. At higher pH, H_2O_2 decomposed rapidly into H_2O and molecular oxygen.[54] Also, because a small amount of Fe_2O_3 impurities in CG-X react with OH^-, it indirectly affects the degradation efficiency. Therefore, the degradation efficiency of methylene blue was reduced under strongly alkaline conditions. Compared to Fe, Cu ions were less sensitive to pH, which meant that Cu-based Fenton systems can operate over a wide range of pH values. This phenomenon made Cu-based Fenton systems more likely to be used in practical applications. Therefore, neutral and near-neutral conditions are favorable for Fenton-like reactions using Cu-X catalysts.

2.3. Recycling of Catalysts. The stability and reproducibility of the CX-1.0 catalyst were examined. The degradation process of methylene blue was repeated several times using the recycled material as the catalyst. As shown in Figure 8, the degradation rate only decreased from 99.7% after the first cycle to 98.5% after the fifth cycle, indicating the high recyclability of the catalyst. After five Fenton-like degradation cycles of methylene blue, XPS analysis showed that the Cu content was reduced by only 0.4%. The catalyst had good reusability, and its structural stability was good because the loss of copper from the system in the reaction was negligible. This indicated that the CX-1.0 catalyst was stable and reusable for the degradation of methylene blue, which is of great value for practical applications.

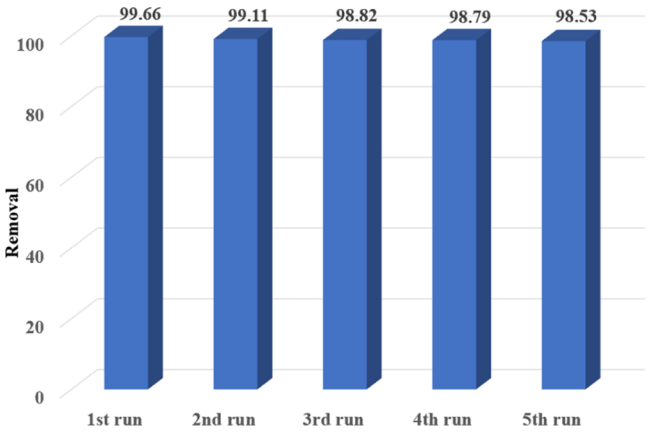

Figure 8. Cycling experiment results for the degradation of methylene blue using the CX-1.0 catalyst.

2.4. Mechanism of the Methylene Blue Degradation Reaction. Reactive radicals generally play an important role in the catalytic Fenton process. To obtain information about the reactive radicals during the degradation of methylene blue by Fenton-like processes, radical capture experiments were performed. Scavengers such as isopropyl alcohol (IPA), benzoquinone (BQ), NaN_3, and KI were added to the reaction system to capture hydroxyl radicals ($^{\bullet}OH$), superoxide radicals ($^{\bullet}O^{2-}$), singlet oxygen ($^1O_2$), and vacancies (h^+), respectively.[38] The results in Figure 9a indicate that the Fenton-like degradation of methylene blue was the result of the synergistic action of Cu and H_2O_2. Figure 9b,c shows that $^{\bullet}OH$ played a dominant role in the degradation of methylene blue and the removal rate of total organic carbon (TOC) in the Fenton-like reaction. To further confirm the capture results, electron spin resonance (ESR) experiments were also performed. Figure 9d shows the ESR of hydroxyl radicals. In the CX-1.0 + H_2O_2 + methylene blue system, all four characteristic peaks of 5,5-dimethyl-1-pyrroline *N*-oxide (DMPO)-$^{\bullet}OH$ adducts appeared with an intensity ratio of 1:2:2:1, indicating the presence of $^{\bullet}OH$ radicals in the system.

These results indicated that the Cu-X + H_2O_2 system had a high catalytic activity for the degradation of methylene blue. The possible mechanism of methylene blue degradation is shown in Figure 10. The XPS results indicated the presence of both Cu^+ and Cu^{2+} in the CX-1.0 catalyst. The presumed reaction mechanism is shown in eqs 6−12, where Me denotes the metal cation, Cu^{2+} and Cu^+, on the surface of the material and MB denotes methylene blue. First, methylene blue was adsorbed on the surface of the Cu-X catalyst (eq 6). Then, when H_2O_2 was added to the reaction system, Cu^{2+} on the catalyst surface reacted with H_2O_2 to form $^{\bullet}OOH$ (eq 7). H_2O_2 reacted with Cu^+ to form Cu^{2+} and $^{\bullet}OH$ (eq 8). The presence of an acid−base equilibrium (eq 9) continued to produce $^{\bullet}O^{2-}$ radicals, some of which reacted with $^{\bullet}OOH$ to form H_2O_2 (eq 10), while others reacted with H_2O_2 to form the strongly oxidizing $^{\bullet}OH$ radical (eq 11). Eventually, methylene blue adsorbed on the catalyst surface was decomposed by $^{\bullet}OH$. Methylene blue was further oxidized by reactive radicals to produce various organic aldehydes, alcohols,[55] and finally CO_2 and H_2O (eq 12). In conclusion, $^{\bullet}OH$ was the main reactive radical, and the redox cycle of Cu^+/Cu^{2+} accelerated the generation of reactive radicals in the Fenton-like system and promoted the degradation of methylene blue.

$$MeOH^+ + MB \rightarrow MeOMB + H^+ \quad (6)$$

$$Cu^{2+} + H_2O_2 \rightarrow Cu^+ + H^+ + {}^{\bullet}OOH \quad (7)$$

$$Cu^+ + H_2O_2 \rightarrow Cu^{2+} + OH^- \quad (8)$$

$$^{\bullet}OOH \rightarrow {}^{\bullet}O_2^- + H^+ \quad (9)$$

$$^{\bullet}O_2^- + {}^{\bullet}OOH \rightarrow H_2O_2 + O_2 \quad (10)$$

$$^{\bullet}O_2^- + H_2O_2 \rightarrow O_2 + OH^- + {}^{\bullet}OH \quad (11)$$

$$MeOMB + {}^{\bullet}OH \rightarrow H_2O + CO_2 \quad (12)$$

https://doi.org/10.1021/acsomega.1c02469
ACS Omega 2021, 6, 18414−18425

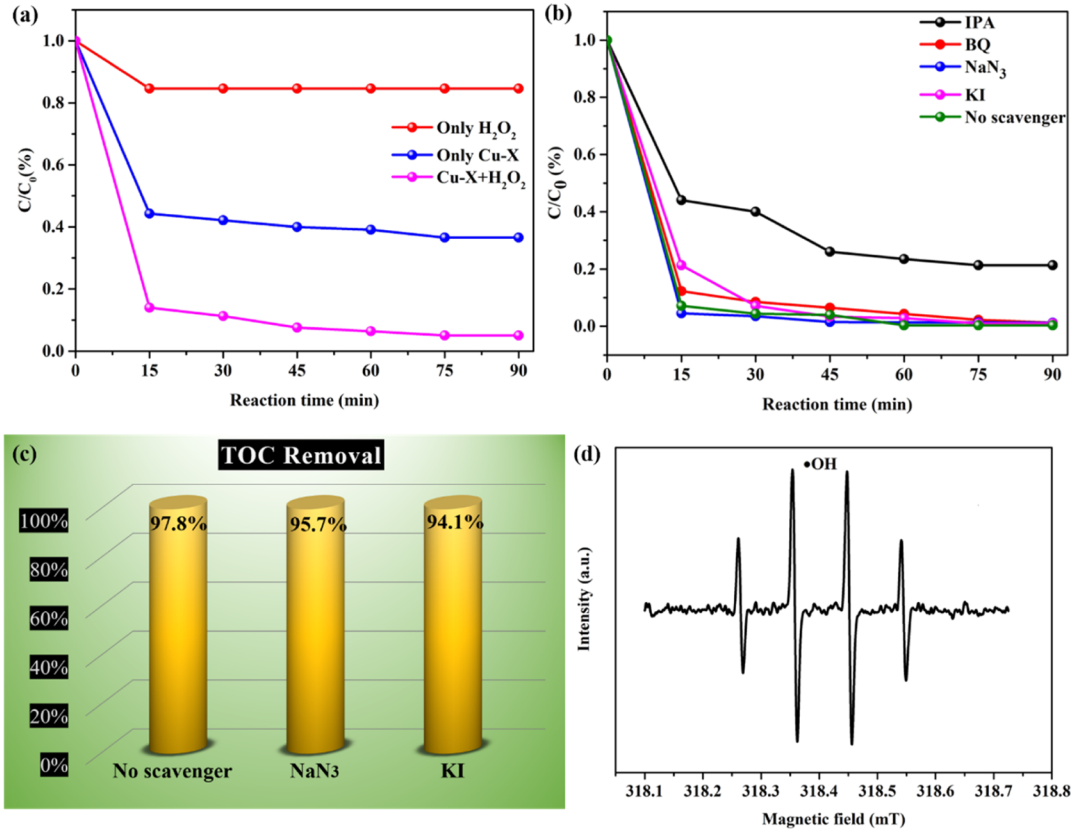

Figure 9. Degradation of methylene blue in Cu-X, H_2O_2, and CX-1.0 + H_2O_2 systems. (a) Effect of IPA, BQ, NaN_3, and KI on the methylene blue degradation efficiency of CX-1.0. (b) Effect of NaN_3 and KI on the removal efficiency of TOC (c) and DMPO-$^{\bullet}$OH (CX-1.0 + H_2O_2 system) ESR spectrum (d).

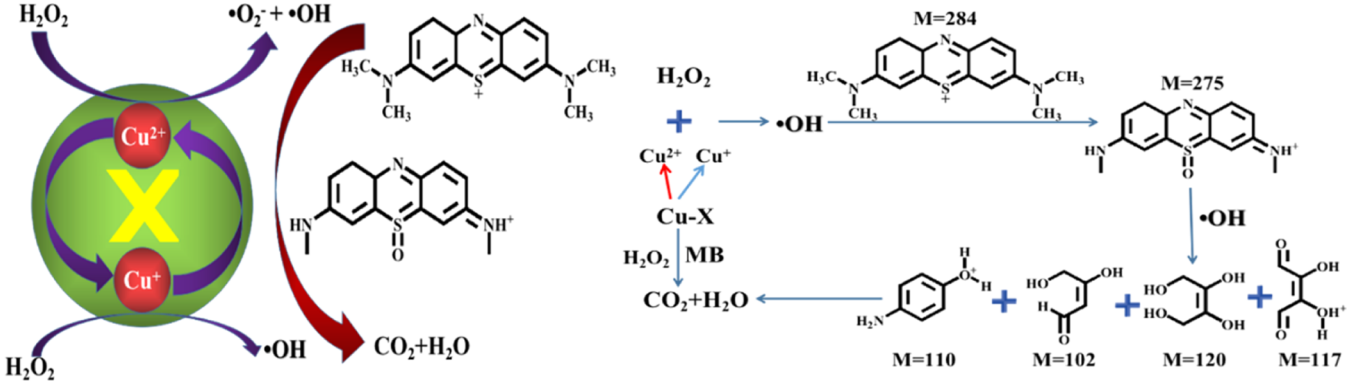

Figure 10. Possible mechanism of the Fenton-like reaction using CX-1.0 to promote the degradation of methylene blue.

3. CONCLUSIONS

A series of Cu-modified X-type zeolite molecular sieve (Cu-X) catalysts were synthesized by an impregnation calcination method using coal gangue as the raw material. The following conclusions were drawn.

(1) An X-type zeolite was synthesized using coal gangue, and Cu-X catalysts with different copper contents were synthesized by an impregnation calcination method. Cu is considered to be present in the surface structure of the zeolite in the form of doped Cu ions and metal oxide. Also, because CG-X has a larger specific surface area, it can load more Cu^{2+}, which provides more active sites for the Fenton-like reaction and indirectly improves the catalytic activity of the Fenton reaction.

(2) The obtained Cu-X catalysts have good catalytic activity for the dye methylene blue. The catalytic degradation rate was up to 99.7% and the TOC removal rate was up to 97.8% at a dye concentration of 100 mg/L at 60 °C, with pH ranging from 7 to 10, 4% copper loading, 1.0 g/L catalyst dosage, and 1.5 mL of H_2O_2. The catalysts had good recyclability.

(3) Fenton-like degradation of methylene blue was the result of the synergistic action between Cu and H_2O_2. $^{\bullet}$OH was the main reactive radical, and the redox cycle of Cu^{+}/Cu^{2+} accelerated the generation of reactive radicals in the Fenton-like system, which promoted the degradation of methylene blue.

https://doi.org/10.1021/acsomega.1c02469
ACS Omega 2021, 6, 18414−18425

4. EXPERIMENTAL SECTION

4.1. Reagents and Materials. The coal gangue was obtained from the Yakeshi Free River Coal Mine, Hulunbeier City, Inner Mongolia, China, and the chemical composition is shown in Table 1. $Cu(NO_3)_2{\cdot}3H_2O$ (AR) was purchased from the Tianjin Sinopharm Chemical Reagent Company, China. H_2O_2 (30 wt %) (AR) was purchased from the Tianjin Damao Chemical Reagent Factory, China. Cetyl trimethyl ammonium bromide (CTAB) (AR) was purchased from the Tianjin Guangfu Fine Chemical Research Institute, China. Methylene blue (AR) was purchased from the Tianjin Yongsheng Fine Chemical Company, China.

4.2. Sample Preparation. The main chemical components are shown in Table 2. It can be seen from the table that

Table 2. Main Chemical Composition of Coal Gangue

composition	SiO_2	Al_2O_3	Fe_2O_3	CaO	MgO	Na_2O	LOS
content/%	61.8	19.18	2.62	0.25	0.15	0.57	30.68

$n(SiO_2)/n(Al_2O_3)$ = 5.5 is suitable for preparing the zeolite. The coal gangue was crushed, ball-milled, and then passed through 100 mesh sieves to obtain coal gangue powder (CG). After heating at 850 °C for 4 h in a muffle furnace, roasted coal gangue (rCG) was obtained. Activated coal gangue (rCG) was digested with anhydrous sodium carbonate [m(rCG)/$m(Na_2CO_3)$ = 1:2] under heating at 850 °C for 3 h to obtain a light-green solid sample (hCG). The hCG sample was mixed with a 1 mol/L NaOH solution and prepared into a suspension according to the solid−liquid ratio of 0.11 g/mL; then, a mesoporous templating agent, CTAB, was added [m(hCG)/m(CTAB) = 2:1] and gelatinized under magnetic stirring for 12 h at room temperature. The sample was then transferred to an autoclave for hydrothermal crystallization at 100 °C. The crystallization products were washed with water and ethanol and then dried at 100 °C. The sample was put into a muffle furnace and heated at 500 °C for 4 h. The final sample of the mesoporous X-type zeolite molecular sieve was obtained by removing the templating agent CTAB.

Preparation of Cu-X catalysts: Cu-modified X-type zeolite molecular sieve samples were synthesized by the ion-exchange method using copper nitrate as the metal precursor. 0.1 g of the X-type zeolite was added to 30 mL of 0.5, 0.8, 1.0, and 1.5 g/L copper nitrate solutions, and the suspensions were magnetically stirred at room temperature for 12 h. The resulting suspensions were washed with water, dried at 100 °C, and heated at 500 °C for 4 h. The Cu-modified X-type zeolite catalysts were obtained and marked as CX-0.5, CX-0.8, CX-1.0, and CX-1.5, respectively (Figure 11).

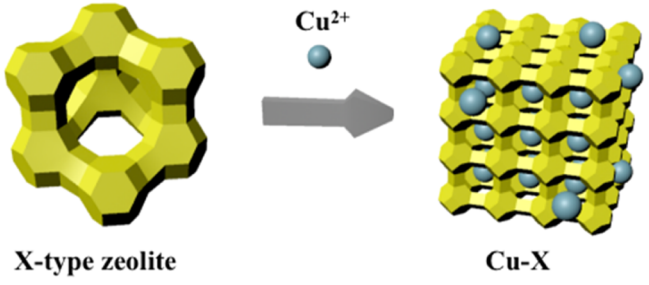

Figure 11. Images of X-type zeolite (left) and X-type zeolite loaded with copper ions(right).

4.3. Characterization Techniques. Infrared spectroscopy (FT-IR) analysis was performed using a 6700 Fourier infrared spectrometer from Nicolet, USA, and characterized by the potassium bromide compression method. The samples were mixed with the reference KBr, pressed into tablets, and tested on the instrument in the wavelength range 400−4000 nm. Powder XRD was performed by using PW1830 from the Beijing Oriental Morning View Technology Company, China, to analyze the morphology of each component in the sample. Test conditions include a Cu tube, a scanning range (2θ) of 5−80°, a scanning speed of 8°/min, a voltage of 40 kW, and a current of 40 mA. An ultraviolet−visible spectrophotometer (UV−vis), METASH UV-5100 from the Shanghai Yuan Analysis Instruments Co., Ltd., was used to detect the change in the concentration of degraded methylene blue. Specific surface testing was performed using an ASAP2020 BET analyzer from Micromeritics, USA, to determine the N_2 isothermal adsorption−desorption curves of the samples at 77 K. The specific surface area and pore size distribution of the samples were analyzed and determined. SEM was performed using a Hitachi S4800 field-emission scanning electron microscope (Japan) with a secondary electron resolution of 1.0 nm (15 kV)/2.0 nm (1 kV) and a backscattered electron resolution of 3.0 nm (15 kV) on a scanning electron microscope with an accelerating voltage of 5.0 kV. The surface morphology of the samples was analyzed on a scanning electron microscope with an acceleration voltage of 5.0 kV. XPS was measured with monochromatized Al Kα radiation ($h\nu$ = 1486.6 eV) using a Thermo Fisher K-α spectrometer (ESCALAB250Xi, Thermo Fisher, USA). The prepared catalysts were analyzed by a transmission electron microscope (JEOL JEM-2100F, Japan) for the microstructure and morphological dimensions. Determination of coal gangue composition was done by the X-ray fluorescence method (AxiosmAX, PANalytical). The TOC content was determined by a TOC analyzer (Elementar, Vario TOC, Germany). ESR measurements were carried out on a JEOLJESFA200 spectrometer. The $^{\bullet}OH$ radical was determined by capturing the radical signal with DMPO.

4.4. Fenton-like Catalytic Degradation of Methylene Blue. The adsorption and catalytic oxidative degradation experiments of MB were carried out in a beaker containing 100 mL of a 100 mg/L MB solution under constant temperature and stirring conditions. 0.1 g of the catalyst was dispersed in the MB solution (100 mg/L), while 1.5 mL of a 30% H_2O_2 solution was added to start the Fenton-like reaction. Hydrochloric acid (1 mol/L) and sodium hydroxide solution (1 mol/L) were used to adjust the pH value of the solution. The effects of different parameters on the degradation efficiency of MB were examined. The degradation rate of MB was tested by a UV spectrophotometer, with the degradation degree $\eta = (C_0 - C_t)/C_0$, where C_t is the concentration of MB at a given moment and C_0 is the starting concentration of MB. The degree of mineralization was derived from the TOC test, and the removal rate was calculated by $\eta = (T_0 - T_t)/T_0$, where T_t is the total organic carbon content within at a certain moment and T_0 is the total organic carbon content at the beginning.

In this experiment, the conditions of copper loading, dosing amount, dye concentration, solution pH, reaction temperature, and H_2O_2 dosage were optimized. The optimal catalytic conditions were determined, and the catalytic mechanism was investigated.

https://doi.org/10.1021/acsomega.1c02469
ACS Omega 2021, 6, 18414−18425

AUTHOR INFORMATION

Corresponding Author

XiaoLi Wang − *Inner Mongolia Key Laboratory of Environmental Chemistry, College of Chemistry and Environmental Science, Inner Mongolia Normal University, Hohhot 010022, China;* orcid.org/0000-0003-3593-4316; Phone: 0471-4392442; Email: hxxwangxiaoli@163.com

Author

MiaoSen Zhang − *Inner Mongolia Key Laboratory of Environmental Chemistry, College of Chemistry and Environmental Science, Inner Mongolia Normal University, Hohhot 010022, China*

Complete contact information is available at: https://pubs.acs.org/10.1021/acsomega.1c02469

Notes

The authors declare no competing financial interest.

ACKNOWLEDGMENTS

This work was supported by the National Natural Science Foundation of China under the project Synthesis of zeolite-based adsorbent from coal gangue in Inner Mongolia and its adsorption performance (21567020) and the Collaborative Innovation Center for Water Environmental Security of Inner Mongolia Autonomous Region, China (XTCX003).

REFERENCES

(1) Huang, Z.; Le, T.; Zhang, Y.; Gao, Y.; Li, J.; Li, Z.; Ma, Z. Development and performance study of a novel physicochemical composite inhibitor for the prevention of coal gangue spontaneous combustion. *Fire Mater.* **2020**, *44*, 76−89.

(2) Liang, L.; Xu, X.; Han, J.; Xu, Z.; Wu, P.; Guo, J.; Qiu, G. Characteristics, speciation, and bioavailability of mercury and methylmercury impacted by an abandoned coal gangue in southwestern China. *Environ. Sci. Pollut. Res.* **2019**, *26*, 37001−37011.

(3) Ge, Q.; Moeen, M.; Tian, Q.; Xu, J.; Feng, K. Highly effective removal of Pb^{2+} in aqueous solution by Na-X zeolite derived from coal gangue. *Environ. Sci. Pollut. Res.* **2020**, *27*, 7398−7408.

(4) Ahmed, I.; Jhung, S. H. Applications of metal-organic frameworks in adsorption/separation processes via hydrogen bonding interactions. *Chem. Eng. J.* **2017**, *310*, 197−215.

(5) Wen, J.; Fang, Y.; Zeng, G. Progress and prospect of adsorptive removal of heavy metal ions from aqueous solution using metal-organic frameworks: A review of studies from the last decade. *Chemosphere* **2018**, *201*, 627−643.

(6) Han, L.-J.; Ge, F.-Y.; Sun, G.-H.; Gao, X.-J.; Zheng, H.-G. Effective adsorption of Congo red by a MOF-based magnetic material. *Dalton Trans.* **2019**, *48*, 4650−4656.

(7) Mantasha, I.; Shahid, M.; Saleh, H.; Qasem, K.; Ahmad, M. A novel sustainable metal organic framework as the ultimate aqueous phase sensor for natural hazards: detection of nitrobenzene and f at the ppb level and rapid and selective adsorption of methylene blue. *CrystEngComm* **2020**, *22*, 3891−3909.

(8) Tang, J.; Wang, J. Fenton-like degradation of sulfamethoxazole using Fe-based magnetic nanoparticles embedded into mesoporous carbon hybrid as an efficient catalyst. *Chem. Eng. J.* **2018**, *351*, 1085−1094.

(9) Tang, L.; Xiao, F.; Wei, Q.; Liu, Y.; Zou, Y.; Liu, J.; Sand, W.; Chow, C. Removal of active dyes by ultrafiltration membrane pre-deposited with a PSFM coagulant: Performance and mechanism. *Chemosphere* **2019**, *223*, 204−210.

(10) Zang, C.; Zhang, X.; Hu, S.; Chen, F. The role of exposed facets in the Fenton-like reactivity of CeO_2 nanocrystal to the Orange II. *Appl. Catal., B* **2017**, *216*, 106−113.

(11) Jiang, Y.; Gao, J.; Zhang, Q.; Liu, Z.; Fu, M.; Wu, J.; Hu, Y.; Ye, D. Enhanced Oxygen Vacancies to Improve Ethyl Acetate Oxidation Over MnOx-CeO_2 Catalyst Derived from MOF Template. *Chem. Eng. J.* **2019**, *371*, 78−87.

(12) Hu, P.; Zhao, Z.; Sun, X.; Muhammad, Y.; Li, J.; Chen, S.; Pang, C.; Liao, T.; Zhao, Z. Construction of crystal defect sites in N-coordinated UiO-66 via mechanochemical in-situ N-doping strategy for highly selective adsorption of cationic dyes. *Chem. Eng. J.* **2019**, *356*, 329−340.

(13) Sonkusare, V. N.; Chaudhary, R. G.; Bhusari, G. S.; Mondal, A.; Potbhare, A. K.; Mishra, R. K.; Juneja, H. D.; Abdala, A. A. Mesoporous Octahedron-Shaped Tricobalt Tetroxide Nanoparticles for Photocatalytic Degradation of Toxic Dyes. *ACS Omega* **2020**, *5*, 7823−7835.

(14) Hodges, B. C.; Cates, E. L.; Kim, J.-H. Challenges and prospects of advanced oxidation water treatment processes using catalytic nanomaterials. *Nat. Nanotechnol.* **2018**, *13*, 642−650.

(15) Nguyen, X. S.; Zhang, G.; Yang, X. Mesocrystalline Zn-doped Fe_3O_4 hollow submicrospheres: formation mechanism and enhanced photo-Fenton catalytic performance. *ACS Appl. Mater. Interfaces* **2017**, *9*, 8900−8909.

(16) Chen, Y.; Zhang, G.; Liu, H.; Qu, J. Confining free radicals in close vicinity to contaminants enables ultrafast Fenton-like processes in the interspacing of MoS_2 membranes. *Angew. Chem. Int. Ed.* **2019**, *58*, 8134−8138.

(17) Song, Q.; Feng, Y.; Liu, G.; Lv, W. Degradation of the flame retardant triphenyl phosphate by ferrous ion-activated hydrogen peroxide and persulfate: Kinetics, pathways, and mechanisms. *Chem. Eng. J.* **2019**, *361*, 929−936.

(18) Li, X.; Huang, X.; Xi, S.; Miao, S.; Ding, J.; Cai, W.; Liu, S.; Yang, X.; Yang, H.; Gao, J.; et al. Single cobalt atoms anchored on porous N-doped graphene with dual reaction sites for efficient Fenton-like catalysis. *J. Am. Chem. Soc.* **2018**, *140*, 12469−12475.

(19) Du, J.; Bao, J.; Fu, X.; Lu, C.; Kim, S. H. Mesoporous sulfur-modified iron oxide as an effective Fenton-like catalyst for degradation of bisphenol A. *Appl. Catal., B* **2016**, *184*, 132−141.

(20) Clarizia, L.; Russo, D.; Di Somma, I.; Marotta, R.; Andreozzi, R. Homogeneous photo-Fenton processes at near neutral pH: A review. *Appl. Catal., B* **2017**, *209*, 358−371.

(21) Xing, M.; Xu, W.; Dong, C.; Bai, Y.; Zeng, J.; Zhou, Y.; Zhang, J.; Yin, Y. Metal sulfides as excellent co-catalysts for H_2O_2 decomposition in advanced oxidation processes. *Chemosphere* **2018**, *4*, 1359−1372.

(22) Liu, J.; Du, Y.; Ye, T.; Cao, J.; Peng, C. Removal of Orange II using an adsorbent-supported zero-valent iron as a heterogeneous Fenton-like catalyst. *Desalin. Water Treat.* **2020**, *175*, 273−281.

(23) Reyhani, A.; Mazaheri, O.; Alivand, M. S.; Mumford, K. A.; Qiao, G. Temporal Control of RAFT Polymerization via Magnetic Catalysis. *Polym. Chem.* **2020**, *11*, 2838−2846.

(24) Li, X.; Xiao, B.; Wu, M.; Wang, L.; Chen, R.; Wei, Y.; Liu, H. In-situ generation of multi-homogeneous/heterogeneous Fe-based Fenton catalysts toward rapid degradation of organic pollutants at near neutral pH. *Chemosphere* **2020**, *245*, 125663.

(25) Liu, Y.; Jin, W.; Zhao, Y.; Zhang, G.; Zhang, W. Enhanced catalytic degradation of methylene blue by alpha-Fe_2O_3/graphene oxide via heterogeneous photo-Fenton reactions. *Appl. Catal., B* **2017**, *206*, 642−652.

(26) Zhang, N.; Chen, J.; Fang, Z.; Tsang, E. P. Ceria accelerated nanoscale zerovalent iron assisted heterogenous Fenton oxidation of tetracycline. *Chem. Eng. J.* **2019**, *369*, 588−599.

(27) Cheng, M.; Zeng, G.; Huang, D.; Lai, C.; Liu, Y.; Zhang, C.; Wan, J.; Hu, L.; Zhou, C.; Xiong, W. Efficient degradation of sulfamethazine in simulated and real wastewater at slightly basic pH values using Co-SAM-SCS/H_2O_2 Fenton-like system. *Water Res.* **2018**, *138*, 7−18.

(28) Niaei, H. A.; Rostamizadeh, M. Adsorption and electro-Fenton processes over FeZSM-5 nano-zeolite for tetracycline removal from wastewater. *Adv. Nano Res.* **2020**, *9*, 173−181.

(29) Adityosulindro, S.; Carine, J.; Laurie, B. Heterogeneous Fenton oxidation using Fe-ZSM5 catalyst for removal of ibuprofen in wastewater. *J. Environ. Chem. Eng.* **2018**, *6*, 5920−5928.
(30) Garcia-Muñoz, P.; Fresno, F.; Lefevre, C.; Rebert, D.; Keller, N. Synergy effect between photocatalysis and heterogeneous photo-Fenton catalysis on Ti-doped $LaFeO_3$ perovskite for high efficiency light-assisted water treatment. *Catal. Sci. Technol.* **2020**, *10*, 1299−1310.
(31) Phan, T. T. N.; Nikoloski, A. N.; Bahri, P. A.; Li, D. Heterogeneous photo-Fenton degradation of organics using highly efficient Cu-doped $LaFeO_3$ under visible light. *J. Ind. Eng. Chem.* **2018**, *61*, 53−64.
(32) Dos Santos, A. J.; Sires, I.; Alves, A. P. M.; Martinez-Huitle, C. A.; Brillas, E. Vermiculite as heterogeneous catalyst in electrochemical Fenton- based processes: Application to the oxidation of Ponceau SS dye. *Chemosphere* **2020**, *240*, 124838.
(33) Zhou, S.; Xu, R.; He, J.; Huang, Y.; Cai, Z.; Xu, M.; Song, Z. Preparation of Fe-Cu-kaolinite for catalytic wet peroxide oxidation of 4-chlorophenol. *Environ. Sci. Pollut. Res.* **2018**, *25*, 4924−4933.
(34) Wang, Q.; Ma, Y.; Xing, S. Comparative study of Cu-based bimetallic oxides for Fenton-like degradation of organic pollutants. *Chemosphere* **2018**, *203*, 450−456.
(35) Zhang, C.; Wang, Y.; Li, G.; Chen, L.; Zhang, Q.; Wang, D.; Li, X.; Wang, Z. Tuning smaller Co_3O_4 nanoparticles onto HZSM-5 zeolite via complexing agents for boosting toluene oxidation performance. *Appl. Surf. Sci* **2020**, *532*, 147320.
(36) Zhang, C.; Huang, H.; Li, G.; Wang, L.; Song, L.; Li, X. Zeolitic acidity as a promoter for the catalytic oxidation of toluene over MnOx/HZSM-5 catalysts. *Catal. Today* **2019**, *327*, 374−381.
(37) Lu, S.; Liu, Q.; Han, R.; Shi, J.; Guo, M.; Song, C.; Ji, N.; Lu, X.; Ma, D. Core-shell structured Y zeolite/hydrophobic organic polymer with improved toluene adsorption capacity under dry and wet conditions. *Chem. Eng. J.* **2021**, *409*, 128194.
(38) Li, H.; Cheng, R.; Liu, Z.; Du, C. Waste control by waste: Fenton−like oxidation of phenol over Cu modified ZSM−5 from coal gangue. *Sci. Total Environ.* **2019**, *683*, 638−647.
(39) Huang, C.; Hu, J.; Cong, S.; Zhao, Z.; Qiu, X. Hierarchical BiOCl microflowers with improved visible-light-driven photocatalytic activity by Fe (III) modification. *Appl. Catal., B* **2015**, *174-175*, 105−112.
(40) Liu, Y.; Song, C.; Lv, G.; Fan, C.; Li, X. Promotional Effect of cerium and/or zirconium doping on Cu/ZSM-5 catalysts for selective catalytic reduction of NO by NH_3. *Catalysts* **2018**, *8*, 306.
(41) Alvarez-García, S.; Guadalupe, M. M.; Sonia, M. G.; Eduardo, O. R.; Jessica, L. C.; Enrique, A. M. Removal of triclosan by CTAB-modified zeolite-rich tuff from aqueous solutions. *MRS Adv.* **2020**, *5*, 3257−3264.
(42) Zhou, J.; Zheng, F.; Li, H.; Wang, J.; Bu, N.; Hu, P.; Gao, J.; Zhen, Q.; Bashir, S.; Liu, L. Optimization of post-treatment variables to produce hierarchical porous zeolites from coal gangue to enhance adsorption performance. *Chem. Eng. J.* **2020**, *381*, 122698.
(43) Faheem, M.; Jiang, X.; Wang, L.; Shen, J. Synthesis of Cu_2O-$CuFe_2O_4$ microparticles from Fenton sludge and its application in the Fenton process: the key role of Cu_2O in the catalytic degradation of phenol. *RSC Adv.* **2018**, *8*, 5740−5748.
(44) Zhou, S.; Liu, Y.; Li, J.; Wang, Y.; Jiang, G.; Zhao, Z.; Wang, D.; Duan, A.; Liu, J.; Wei, Y. Facial in situ synthesis of graphitic carbon nitride (g-C_3N_4)-N-TiO_2 heterojunction as an efficient photocatalysts for the selective photoreduction of CO_2 to CO. *Appl. Catal., B* **2014**, *158-159*, 20−29.
(45) Xing, Y.; Gao, X.; Ji, G.; Liu, Z.; Du, C. Synthesis of carbon doped Bi_2MoO_6 for enhanced photocatalytic performance and tumor photodynamic therapy efficiency. *Appl. Surf. Sci.* **2019**, *465*, 369−382.
(46) Wang, y.; Du, T.; Jia, H.; Qiu, Z.; Song, Y. Synthesis characterization and CO_2 adsorption of NaA, NaX and NaZSM-5 from rice husk ash. *Solid State Sci.* **2018**, *86*, 24−33.
(47) Cui, Y.; Zheng, Y.; Wang, W. Synthesis of 4A zeolite from kaolinite-type pyrite flotation tailings (KPFT). *Minerals* **2018**, *8*, 338.
(48) Abdelrahman, E. A. Synthesis of zeolite nanostructures from waste aluminum cans for efficient removal of malachite green dye from aqueous media. *J. Mol. Liq.* **2018**, *253*, 72−82.
(49) Qiang, Z.; Shen, X.; Guo, M.; Cheng, F.; Zhang, M. A simple hydrothermal synthesis of zeolite X from bauxite tailings for highly efficient adsorbing CO_2 at room temperature. *Microporous Mesoporous Mater.* **2019**, *287*, 77−84.
(50) Zhang, J.; Zhang, X.; Wang, Y. Degradation of phenol by a heterogeneous photo-Fenton process using Fe/Cu/Al catalysts. *RSC Adv.* **2016**, *6*, 13168−13176.
(51) Zheng, C.; Yang, C.; Cheng, X.; Xu, S.; Fan, Z.; Wang, G.; Wang, S.; Guan, X.; Sun, X. Specifically enhancement of heterogeneous Fenton-like degradation activities for ofloxacin with synergetic effects of bimetallic Fe-Cu on ordered mesoporous silicon. *Sep. Purif. Technol.* **2017**, *189*, 357−365.
(52) Liang, X.; Zhong, Y.; He, H.; Yuan, P.; Zhu, J.; Zhu, S.; Jiang, Z. The application of chromium substituted magnetite as heterogeneous Fenton catalyst for the degradation of aqueous cationic and anionic dyes. *Chem. Eng. J.* **2012**, *191*, 177−184.
(53) Xia, M.; Long, M.; Yang, Y.; Chen, C.; Cai, W.; Zhou, B. A highly active bimetallic oxides catalyst supported on Al-containing MCM-41 for Fenton oxidation of phenol solution. *Appl. Catal., B* **2011**, *110*, 118−125.
(54) Hu, M.; Xu, Y. Visible light induced degradation of chlorophenols in the presence of H_2O_2 and ion substituted polyoxotungstate. *Chem. Eng. J.* **2014**, *246*, 299−305.
(55) Ma, C.; Feng, S.; Zhou, J.; Chen, R.; Wei, Y.; Liu, H.; Wang, S. Enhancement of H_2O_2 Decomposition Efficiency by the Co-Catalytic Effect of Iron Phosphide on the Fenton Reaction for the Degradation of Methylene Blue. *Appl. Catal., B* **2019**, *259*, 118015.

https://doi.org/10.1021/acsomega.1c02469
ACS Omega 2021, 6, 18414−18425